RSC Advances

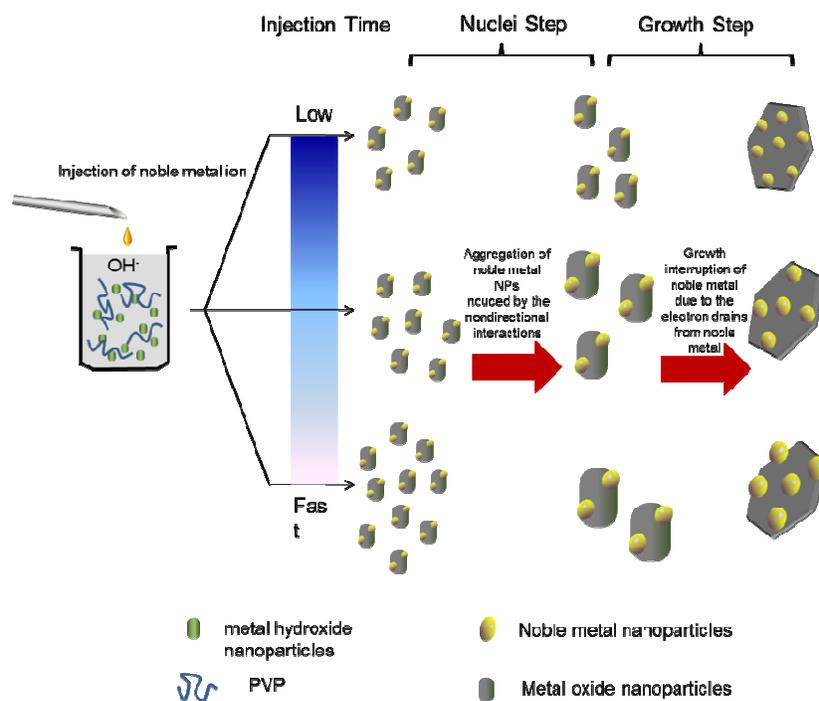# One-step Synthesis of Noble Metal/ Oxide Nanocomposites with Tunable Size of Noble Metal Particles and Their Size-dependent Catalytic Activity

SCHOLARONE™
Manuscripts

A general one-step synthesis for noble metal/oxide nanocomposites with tunable size of noble metal particles and size-dependent catalytic activity

ARTICLE TYPE

One-step Synthesis of Noble Metal/ Oxide Nanocomposites with Tunable Size of Noble Metal Particles and Their Size-dependent Catalytic Activity†

Jie Liu, [ab] Wei Wang, [b] Tong Shen, [b] Zhiwei Zhao,[*ab] Hui Feng, [b] Fuyi Cui[*b]

Synthesis of the noble metal/ oxide nanocomposites with a facile method is still essential and needed. This article demonstrated a general one-step strategy for the synthesis of
10 **noble metal/ oxide nanocomposites in an aqueous route by the means of the reaction between the metal hydroxide and noble metal ion. $Pd-CeO_2$, $Au-Fe_3O_4$ and $Ag-Mn_3O_4$ nanocomposites were fabricated as examples, revealing the generality of the synthesis method. The noble metal**
15 **nanoparticles are tunable in size achieved through the adjustment of the injection rate of the solution containing noble metal ions rather than changing the loading of noble metal. We propose a mechanism for the size variation of the noble metal nanoparticles with the injection rate of the noble**
20 **metal ion solution. The as-synthesized nanocomposites had a stable structure and high yield (>98%) of noble metal. Both of the synthesis and size-control methods can be extended to other nanocomposites preparation. In addition, all of the as-synthesized nanocomposites exhibited superior catalytic**
25 **activities dependent on the size of active metal particle for hydrogenation reactions in aqueous solution.**

Introduction

The past several decades have witnessed the big progress on fabricating noble metal/ oxide nanocomposites with direct
30 conjunction structure for their widely application as heterogeneous catalysts in energy processing, chemical production, environmental remediation, and so on.[1-4] They display superior catalytic performances compared to their single counterparts,[5] due to the synergetic effect caused by the change of
35 the local electronic structure at interface of metal and oxide supports.[6] It is also reported that the catalytic activity of noble metal is highly related to the size of noble metal particles. [7] Therefore, preparation strategy with simple operation and low cost for metal/oxide nanocomposites with direct conjunction
40 between the two components as well as tunable metal particle sizes is highly desired.

Many synthesis methods have been developed for the preparation of the noble metal/oxide composites. Among them, deposition–precipitation (DP) method is a frequently used
45 method, which is based on the transformation of deposited metal hydroxide embryos on the surface of synthesized metal oxide.[8, 9]

The incipient wetness impregnation method is also a common method that is achieved through reducing the pre-absorbed metal precursor on the metal oxide by some reductants under
50 calcination.[10] However, for both of the methods, it is difficult to control the size of noble metal NPs conveniently and to achieve a high yield of noble metal. Epitaxial growth of metal oxide on noble metal seed particles in no polar or low polar solvent is another widely employed strategy in fabrication of asymmetry
55 noble metal/ oxide nanocomposites. The transition metal based organometallic species [11-14] was commonly used as the precursors for generation of metal oxide through their thermal decomposition, and then grown on the surface of the noble metal seed. Nevertheless, the strictly-required phase transfer in aqueous
60 solution, use of the expensive reagents, multistep process and high synthesis temperature are the main drawbacks of the method.[15]

In recent years, one-step methods have attracted much research attention with the advantages of simplicity, low cost and so on in
65 the synthesis of organic molecules[16], organic/inorganic hybrids[17] and carbon based materials. [18] But for noble metal/oxide nanocomposites, it seems to suffer from the difficulty to achieve low cost, environmental friendly synthesis. [19-21]

In this report, using $Pd-CeO_2$, $Au-Fe_3O_4$ and $Ag-Mn_3O_4$ as
70 examples, we propose a simple and general one-step route for the synthesis of noble metal/ oxide nanocomposites in aqueous solution by means of the redox reaction between the metal hydroxide and noble metal ion. The regulating of the noble metal nanoparticles size is conveniently achieved by adjusting of the
75 injection rate of the reaction solution, which is quite different from previous reported method by changing the loading of noble metal. The present work has several unique advantages in comparison with previous noble metal/ oxide nanocomposites fabrication process including a single synthesis step, less use of
80 the reagent, high yield (>98%) and universality. Significantly, the fabricated nanocomposites demonstrated very high and well-defined size dependent catalytic activities towards reduction of 4-nitrophenol.

Experimental

85 **Materials.** Palladium chloride ($PdCl_2$, analytical grade), Chloroauric acid hydrated ($HAuCl_4·4H_2O$, analytical grade),

cerium (III) nitrate hexahydrate (Ce(NO$_3$)$_3$·6H$_2$O, analytical grade), ferrous sulfate hydrate (FeSO$_4$·7H$_2$O, analytical grade), manganese(II) chloride tetrahydrate (MnCl$_2$·4H$_2$O, analytical grade), silver nitrate (AgNO$_3$, analytical grade), sodium
5 hydroxide (NaOH, analytical grade), and polyvinylpyrrolidone (PVP K30, analytical grade) were all purchased from Sinopharm Chemical Reagent Co. Ltd. (Shanghai, China) without purification.

Synthesis of the Pd-CeO$_2$ Nanocomposites. In a typical
10 synthesis of Pd-CeO$_2$ nanocomposites, Ce(NO$_3$)$_3$·6H$_2$O (1.2 mmol) and poly (vinylpyrrolidone) (PVP, K-30, 1.5 g) were dissolved in 150 mL deionized water (DI water) and kept for 1 h under N$_2$ protection. And then, 1 mL of 5.0 M NaOH was added into the mixture. After 5 min, 30 mL of Pd^{2+} solution (containing
15 0.4 mmol Pd^{2+} and 0.3 g PVP) was added into the reaction solution immediately or injected by means of the peristaltic pump with injection time at 20 min and 50 min, referred to as Pd-Ce1, Pd-Ce20 and Pd-Ce50, respectively. Next, the generated black precipitate was aged with the mother liquid for 6 h and were
20 washed six times using DI water and ethanol alternately, followed by drying in a vacuum drying oven at 323 K.

Synthesis of the Au-Fe$_3$O$_4$ and Ag-Mn$_3$O$_4$ Nanocomposites. For Au-Fe$_3$O$_4$, the usage of FeSO$_4$·7H$_2$O was 1 mmol and HAuCl$_4$·4H$_2$O was 0.1 mmol. Au-Fe1, Au-Fe5 and Au-Fe30
25 refer to the samples prepared by rapid one-time injection, injection in 5 mins and 30-mins, respectively. While for the synthesis of Ag-Mn$_3$O$_4$, 1 mmol of MnCl$_2$·4H$_2$O and 0.2 mmol of AgNO$_3$ were used. The other synthesis steps and conditions are same to the synthesis of Pd-CeO$_2$ nanocomposites.

30 **Materials Characterizations.** XRD patterns of as-synthesized samples were acquired using Cu Kα photons from a diffractometer (Rigaku D/MAX-2000, Japan) operated at 40 kV×30 mA with 2θ ranging from 10° to 90°. Transmission electron microscopy (TEM), high resolution TEM (HRTEM) and
35 high-angle annular dark field scanning transmission electron microscopy (HAADF-STEM) images are acquired using an F-20 (Tecnai) S-Twin microscopy operated at 200 kV with energy dispersive analysis of X-rays (EDAX) and a HAADF detector. The chemical composition of the sample surface was identified
40 by using X-ray photoelectron spectroscopy (XPS; PHI 5700 ESCA System, U.S.). An Analytik Jena Specord 200 UV-vis spectrophotometer (Jena, Germany) is used to measure the concentration change of 4-nitrophenol in a 1 cm path length quartz cuvette over a wavelength range from 200 to 600 nm.

45 **Catalytic Reduction of 4-nitrophenol with Noble Metal/ Oxide Nanocomposites.** 0.15 mL of 4-nitrophenol (1 mM) and 0.15 mL of NaBH$_4$ (0.1 M) were mixed with 2.7 mL water in a quartz cuvette with stirring. After that, 50 μL of the corresponding catalyst (1 mg/mL) was added into the mixture.
50 The concentration change of the 4-nitrophenol was analysed by measuring the UV-vis absorption spectra of the reaction solution at a special time interval.

Results and Discussion

For the synthesis of Pd-CeO$_2$, we added 30 mL Pd^{2+} solution into
55 the heated solution at one time, and the colour of the suspension turned from white to brown and then dark brown, suggesting very fast production of Pd(OH)$_2$ and redox reaction between Pd(OH)$_2$

and Ce(OH)$_3$ **(eqs S1 and S2)**. The morphology of Pd-Ce1 was charactered by TEM. It can be seen from the typical TEM image
60 (Fig. 1a) that rod-like CeO$_2$ NPs attached on the surface of the Pd nanospheres, formatting the nanocomposites structure. When the injection time of Pd^{2+} solution was increased to 20 min and 50 min, the size of the Pd NPs became more unique and smaller, while no change of the CeO$_2$ nanorods (Fig. 1b-c). The histogram
65 analysis calculated from Figures 1a-c showed the average diameters of the Pd NPs were decreased with the increase of the injection time, 30.29 nm, 13.50 nm and 9.45 nm for samples obtained at the injection rate of one time, 20 min and 50 min, respectively.

70 The interfringe distances of Pd-Ce50 showed by HRTEM are measured to be 0.19 nm for Pd nanoparticles corresponding to the (200) plane of face-centered cubic (fcc) Pd, [22] while 0.27 nm for CeO$_2$ nanoparticles keeping with (200) plane of body-centered cubic structured cerium dioxide (Fig. 1g). [23] In addition, the
75 elemental composition of selected areas of Pd-Ce50 was obtained by EDAX (Fig. 1h). Cu, C, Ce and Pd can all be easily found in the EDAX graph. For these elements, Ce and Pd signals result from the CeO$_2$ and Pd particles which form the product.
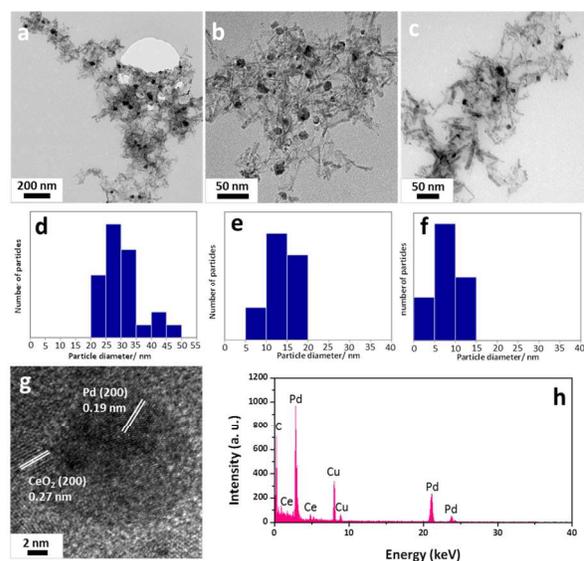

80 **Fig. 1** TEM images of the synthesized Pd-CeO$_2$ nanocomposites: (a) Pd-Ce1, (b) Pd-Ce20 and (c) Pd-Ce50. Histogram analysis of Pd particle size in (d) Pd-Ce1, (e) Pd-Ce20 and (f) Pd-Ce50. (g) HRTEM and (h) EDAX spectrum of the Pd-Ce50. The volume of the all Pd^{2+} solution is 30 mL.

The nanostructure of Pd-CeO$_2$ nanocomposites was examined
85 by the Powder X-ray diffraction (XRD) technology. As seen from the Fig. 2, some peaks can be assigned as the body-centered cubic structured CeO$_2$ and other match well with fcc Pd, which indicated the heterogeneous structure of the nanocomposites. [24] On the other hands, the peak at 40.11° belong to Pd became
90 sharper along with the decrease of the injection time of Pd^{2+} solution, revealing the increase of the size of Pd, [25] which is according with the TEM analysis results.

The oxidation states of Pd and Ce in the Pd-Ce50 were examined by means of the X-ray photoelectron spectroscopy
95 (XPS) analysis. The spectrum of Ce 3d (Fig. 3a) revealed four peaks. Two peaks located at binding energies of 917.0 and 899.6 eV belonged to the Ce^{4+} 3d$_{3/2}$ and Ce^{4+} 3d$_{5/2}$, while others at

905.2 and 884.5 eV for Ce^{3+} $3d_{3/2}$ and Ce^{3+} $3d_{5/2}$, which exhibited the coexistence of Ce^{4+} and Ce^{3+} on the surface of the CeO_2. [26] Pd XPS spectra (Fig. 3b) with Pd $3d_{5/2}$ and Pd $3d_{3/2}$ binding energies of 335.45 and 340.75 eV demonstrated that Pd species in nanocomposites are present in metallic Pd. [27] These results indicate that the occurrence of the redox reaction between Pd^{2+} and $Ce(OH)_3$(eqs S1 and S2).
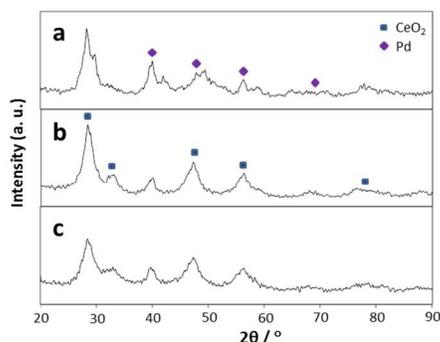

Fig. 2 XRD pattern of the synthesized $Pd-CeO_2$ nanocomposites: (a) Pd-Ce1, (b) Pd-Ce20 and (c) Pd-Ce50.

According to the theoretical stoichiometric ratio, the precursor of Ce was excessive. During the synthesis process, once the reaction between $Ce(OH)_3$ and Pd^{2+} finished, the residual $Ce(OH)_3$ can continue to react with O_2 dissolved in the solution (eqs S3) and generate the metal oxides at the experimental conditions. Zhou *et al.* exposed $Ce(OH)_3$ in the air for 24 h at room temperature and found $Ce(OH)_3$ was partially oxidized. [28] However, in the synthesis process of $Pd-CeO_2$, the residual $Ce(OH)_3$ can be oxidized in 4 hcompletely, which may be induced by the catalysis of Pd for the reaction between $Ce(OH)_3$ and O_2.
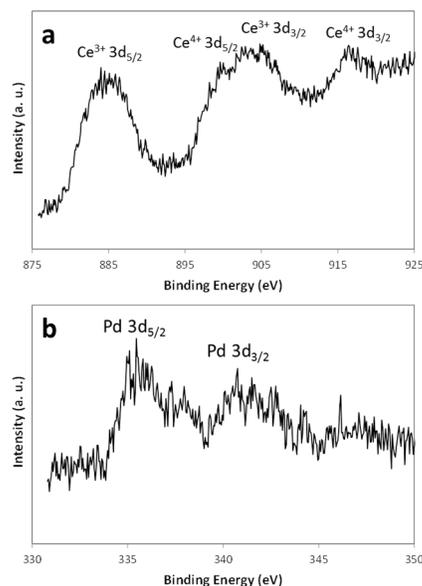

Fig. 3 XPS spectra for (a) Ce 3d (b) Pd 3d of Pd-Ce50.

During the synthesis of $Au-Fe_3O_4$ nanocomposites, the injection time of Au^{3+} solution were one time, 5 min and 30 min. The morphology of the $Au-Fe_3O_4$ nanocomposites is different from the $Pd-CeO_2$ nanocomposites with the same synthesis conditions except injection time. As seen in the TEM and HAADF-STEM images of $Au-Fe_3O_4$ (Fig. 4a-c and Fig. S1), even at the high loading of the noble metal (>20%), sphere like Au NPs highly dispersed on the sheet-like Fe_3O_4 surface. Meanwhile, the size of the noble metal NPs became more unique and smaller along with the increase of the injection time noble metal ion solution, according to the histogram analysis of the Au (Fig. 4d-f) particle size. The HRTEM images and EDAX graph of the Au-Fe30 (Fig. 4g and h) indicated the formation of the composite structure between noble metal and oxide NPs. [29]

XRD spectrum of $Au-Fe_3O_4$ nanocomposites (Fig. S2) showed the peak at 38.18° belong to Au became sharper along with the decrease of the injection time of Au^{3+} solution, revealing the increase of the size of Au, also. XPS analysis of the Au-Fe30 (Fig. S3) revealed the generation of noble metal and oxide, as a results of the redox reactions between the hydroxides of noble metal and oxide precursors (eqs S4 and S5), also. Besides, the residual $Fe(OH)_2$ can be oxidized by O_2 completely to generate Fe_3O_4 (eqs S6). [30]

We also fabricated $Ag-Mn_3O_4$ nanocomposites by this one-step method and studied the effect of the injection time of Ag^+ solution. We can observe the quite similar phenomenon with $Au-Fe_3O_4$, as shown in Fig. S4, Fig. S5, further indicating the generality of the present method.
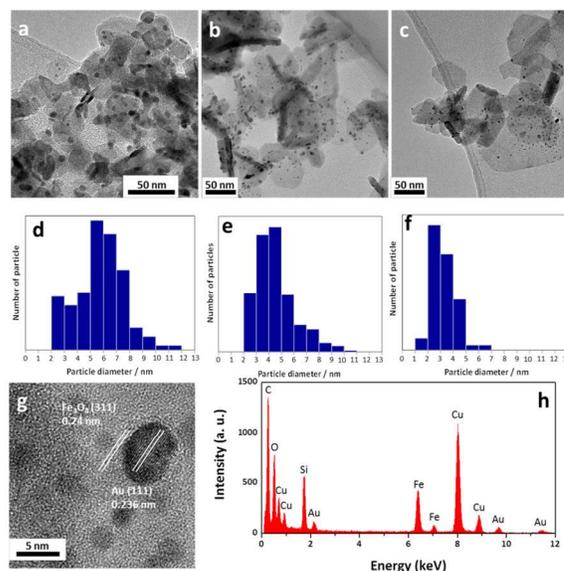

Fig. 4 TEM images of the synthesized $Au-Fe_3O_4$ nanocomposites: (a) Au-Fe1, (b) Au-Fe5 and (c) Au-Fe30. Histogram analysis of Au particle size in (d) Au-Fe1, (e) Au-Fe5 and (f) Au-Fe30. (g) HRTEM and (h) EDAX spectrum of the Au-Fe30. The volume of the all Au^{3+} solution is 30 mL.

In the experiments, we found that all of the nanocomposites have an extremely stable structure, and no noble metal NPs collapsed from the nanocomposites even after 30 min exposure under ultrasonic wave, indicating the strong interaction between noble metal and oxide, which may be induced by the redox reaction of the hydroxides of precursors. Furthermore, no metal ion residue existed in the supernatant after the finish of synthesis, revealing that the yield of the nanocomposites is very high (>98%). In our study, according to the theoretical stoichiometric ratio, the precursors of metal oxide were excessive, so it is easy to

understand the complete conversion of the noble metal ions. On the other hand, once the reaction between metal hydroxide and noble metal finished, the residual metal hydroxide could continue to react with O_2 dissolved in the solution in the mother liquid during the aging process and generated the metal oxides at the experimental conditions.[31, 32] Taking the example of Au-Fe30, the XPS analysis (Fig. S3) revealed the generation of noble metals and oxides, and the residual $Fe(OH)_2$ can be oxidized by O_2 completely to generate Fe_3O_4 (eqs S4).[31] While for Pd-CeO$_2$, researchers have also reported that $Ce(OH)_3$ can be oxidized by air.[32] Additionally, from the XRD pattern of the Pd-Ce50 in Figure 2, a high conversion of the precursor has also been achieved. Although there is Ce (III) observed on the surface of CeO_2, which is likely due to the formation of oxygen vacancies on the surface of ceria. The result is quite similar with that in literature.[26] Therefore, fabrication of nanocomposites with arbitrary mass loading of noble metal below the theoretical value can be achieved easily. Besides, the noble metal particles were dispersed well on the surface of the oxide, although the loading of the noble metal was rather high (Table S1).

Generally speaking, nucleation and growth are the two basic steps during the formation of nanoparticles. [33] In the growth step, larger particles become larger by consuming the smaller particles dissolved in the solvent due to their higher surface free energy. [34] Therefore, a narrow size distribution of the nanoparticles can be obtained through restricting the growth of nanoparticles. [35, 36] For our synthesis process (Fig. 5), in the nucleation step, the generated noble metal and metal oxide NPs formed nuclei rapidly. Meanwhile, strong conjunction of the tow products occurred due to the electrostatic force. After that, the small particles aggregate into larger one mutually induced by the nondirectional interactions, such as van der Waals forces and electrostatic forces as two nanoparticles approach each other closely enough. [37] Moreover, the size of the nuclei has a positive correlation to the noble metal atom concentration gradient in the solution. At a high injection rate of noble metal ion solution, the noble metal atom concentration gradient in solution is higher than low injection rate, resulting in some aggregated Au particles are bigger than one formed at low injection rate. In the growth step, the direct conjunction of the metal oxide and noble metal NPs lead to the electron drains from noble metal and interrupted the growth of noble metal, [28] while no effect on the growth of metal oxide NPs. Therefore, the size control of the noble metal NPs can be achieved by means of the adjustment of the injection time of the noble metal solution, a high injection rate leading to a bigger size and more broad size distribution of noble metal NPs, while no effect on the growth of the metal oxide.
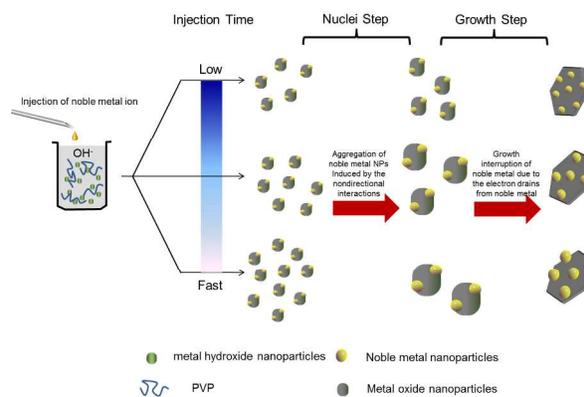

Fig. 5 Schematic depiction of growth mechanism of noble metal/ oxide nanocomposites.

To assess the catalytic activity of the noble metal/ oxide nanocomposites, we study the reduction of 4-nitrophenol by $NaBH_4$ in aqueous solution with noble metal/ oxide nanocomposites as heterogeneous catalysts, a model reaction for the analysis of the catalytic activity of noble metal nanocrystals. [38, 39] The reduction reaction process can be monitored easily and rapidly by means of the UV-vis absorption spectroscopy. In the experiment, the excess $NaBH_4$ in compared with 4-nitrophenol was added in order to make the reduction rate independent to the concentration of $NaBH_4$. The 4-nitrophenol cannot be reduced by $NaBH_4$ in the absence of the catalysts. Moreover, the mixture solution of 4-nitrophenol and $NaBH_4$ has a strong adsorption peak at 400 nm in the UV-vis absorption spectra. Figure 6, as an example, showed the time dependent UV-vis spectral of the reduction reaction of 4-nitrophenol by $NaBH_4$ with Au-Fe30. Upon the addition of the catalysts into the solution, the 4-nitrophenol is reduced, leading to the decrease of the adsorption peak at 400 nm with time and a new peak at 300 nm concomitantly belonging to 4-aminophenol, [40] indicating the conversion of 4- nitrophenol to 4-aminophenol.
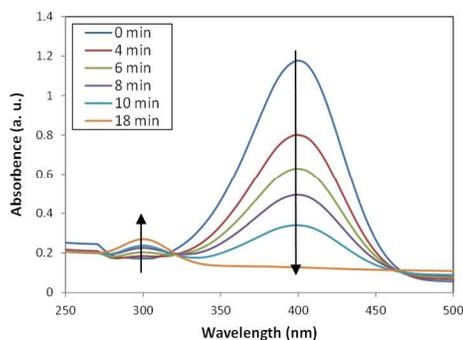

Fig. 6 Time-dependent UV-vis spectral of the reduction reaction of 4-nitrophenol by $NaBH_4$ with Au-Fe30.

In addition, the catalytic activity of all the as-synthesized nanocomposites was tested for the 4-nitrophenol reduction under identical conditions. Fig. 7a, b and Fig. S6 showed the relationship between $\ln(C_t/C_0)$ and reaction time, where the C_t and C_0 were the adsorption peak intensity at time t and 0. The linear relationship of $\ln(C_t/C_0)$ and reaction time revealed that the reactions followed pseudo-first-order kinetics. The reaction rate constants calculated from the Fig. 7a, b and Fig. S6 were listed in

Table S2, demonstrating that the nanocomposites based on Pd-CeO_2, Au-Fe_3O_4 and Ag-Mn_3O_4 had enhanced catalytic activities dependent on the active metal particle size in comparison with previous reports (Table S3), which may be induced by the strong interaction between noble metals and oxides. Moreover, the catalytic activity of the nanocomposites was inversely with the sizes of the active metal particles. In addition, the highest catalytic activity of Pd-CeO_2 nanocomposites may be attribute to the physiochemical character of Pd and the fast electron transfer rate between Pd and CeO_2.
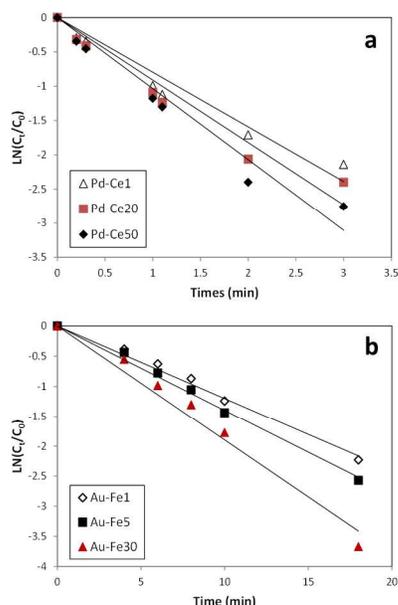

Fig. 7 Linear relationship of $\ln(C_t/C_0)$ with time as a function of time for 4-nitrophenol reduction catalyzed by (a) Pd-CeO_2 nanocomposites and (b) Au-Fe_3O_4 nanocomposites.

Conclusions

In summary, we have developed a novel one-step aqueous approach for the synthesis of the noble metal/ oxide nanocomposites in >98% yield with high stable structure. The size of the noble metal nanoparticles is controlled through the adjustment of the injection time. To the best of our knowledge, this is the first report of the size control of the noble metal in nanocomposites in one-step aqueous route. The noble metal particles dispersed well on the surface of the oxide under high loading of the noble metal. Our method could also be extended to controlled synthesize other types of inorganic/ inorganic or polymer/ inorganic nanocomposites enable to construct heterogeneous nanostructures with novel functionalities. All of the as-synthesized nanocomposites exhibited enhanced and size-dependent catalytic activity for 4-nitrophenol hydrogenation.

Acknowledgements

Notes and references

a. Department of National Defense construction Planning and Environmental Engineering, Logistical Engineering University, Chongqing 401311, China
b. State Key Laboratory of Urban Water Resources and Environments (SKLUWRE) and School of Municipal and Environmental Engineering, Harbin Institute of Technology, Harbin, 150090, China.
E-mail: Fuyi Cui: cuifuyi@hit.edu.cn; Zhiwei Zhao: zhzhw@hit.edu.cn.
† Electronic Supplementary Information (ESI) available: [XRD and XPS spectra of Au-Fe₃O₄ nanocomposites and other results]. See DOI: 10.1039/b000000x/

1 M. Cargnello, J. J. D. Jaén, J. C. H. Garrido, K. Bakhmutsky, T. Montini, J. J. Gámez, C. R. J. Gorte, P. Fornasiero, *Science,* 2012, **337,** 713-717.
2 A. Kim, Y. Won, K. Woo, C. Kim, J. Moon, *ACS Nano,* 2013, **7,** 1081-1091.
3 Z. Jin, M. Xiao, Z. Bao, P. Wang, J. Wang, *Angew. Chem. Int. Ed.,* 2012, **51,** 6406-6410.
4 S. Navalon, M. de Miguel, R. Martin, M. Alvaro, H. Garcia, *J. Am. Chem. Soc.,* 2011, **133,** 2218-2226.
5 W. He, H. Kim, W. G. Wamer, D. Melka, J. H. Callahan, Yin, *J. Am. Chem. Soc.* 2013, **136,** 750-757.
6 C. Xu, J. Xie, D. Ho, C. Wang, N. Kohler, E. G. Walsh, J. R. Morgan, Y. E. Chin, S. Sun, *Angew. Chem. Int. Ed.,* 2008, **47,** 173-176.
7 C. T. Campbell, *Science,* 2004, **306,** 234-235.
8 T. Ishida, N. Kinoshita, H. Okatsu, T. Akita, T. Takei, M. Haruta, *Angew. Chem. Int. Ed.,* 2008, **47,** 9265-9268.
9 M. Shekhar, J. Wang, W.-S. Lee, W. D. Williams, S. M. Kim, E. A. Stach, J. T. Miller, W. N. Delgass, F. H. Ribeiro, *J. Am. Chem. Soc.,* 2012, **134,** 4700-4708.
10 S. Crossley, J. Faria, M. Shen, D. E. Resasco, *Science,* 2010, **327,** 68-72.
11 H. Yu, M. Chen, P. M. Rice, S. X. Wang, R. L. White, S. Sun, *Nano Lett.,* 2005, **5,** 379-382.
12 Y. Zhai, L. Jin, P. Wang, S. Dong, *Chem. Commun.,* 2011, **47,** 8268-8270.
13 S. Chen, R. Si, E. Taylor, J. Janzen, J. Chen, *J. Phys. Chem. C,* 2012, **116,** 12969-12976.
14 Y. Wei, R. Klajn, A. O. Pinchuk and B. A. Grzybowski, *Small,* 2008, **4,** 1635-1639.
15 Y. Zhai, L. Han, P. Wang, G. Li, W. Ren, L. Liu, E. Wang, S. Dong, *ACS Nano,* 2011, **5,** 8562-8570.
16 L. Ye, W. He and L. Zhang, *J. Am. Chem. Soc.,* 2010, **132,** 8550-8851.
17 H. Kong, J. Song and J. Jang, *Chem. Commun.,* 2010, **46,** 6735-6737.
18 S. Sahu, B. Behera, T. K. Maiti and S. Mohapatra, *Chem. Commun.,* 2012, **48,** 8835-8837.
19 Y. Zhang, N. Zhang, Z. Tang, Y. -J. Xu, *ACS Sustainable Chem. Eng.* 2013, **1,** 1258-1266.
20 N. Zhang, Y. -J. Xu, *Chem. Mater.,* 2013, **25,** 1979-1988.
21 M. Yang, X. Pan, N. Zhang, Y. -J. Xu, *CrystEngComm,* 2013, **15,** 6819-6828.
22 R. L. Chantry, I. Atanasov, W. Siriwatcharapiboon, B. P. Khanal, E. R. Zubarev, S. L. Horswell, R. L. Johnston and Z. Y. Li, *Nanoscale,* 2013.
23 W. Song, C. Popa, A. P. J. Jansen and E. J. M. Hensen, *J. Phys. Chem. C,* 2012, **116,** 22904-22915.
24 J. Liu, Z. Zhao, H. Feng, F. Cui, *J. Mater. Chem.,* 2012, **22,** 13891-13894.
25 C. Wang, H. Daimon, S. Sun, *Nano Lett.,* 2009, **9,** 1493-1496.
26 M. Cargnello, M. Grzelczak, B. Rodríguez-González, Z. Syrgiannis, K. Bakhmutsky, V. La Parola, L. M. Liz-Marzán, R. J. Gorte, M. Prato, P. Fornasiero, *J. Am. Chem. Soc.,* 2012, **134,** 11760-11766.
27 G. Ma, A. Binder, M. Chi, C. Liu, R. Jin, D. Jiang, J. Fan and S. Dai, *Chem. Commun.,* 2012, **48,** 11413-11415.
28 K. Zhou, Z. Yang and S. Yang, *Chem. Mater.,* 2007, **19,** 1215-1217.
29 Z. Zhao, J. Liu, F. Cui, H. Feng, L. Zhang, *J. Mater. Chem.,* 2012, **22,** 9052-9057.
30 K. C. Chin, G. L. Chong, C. K. Poh, L. H. Van, C. H. Sow, J. Lin and A. T. S. Wee, *J. Phys. Chem. C,* 2007, **111,** 9136-9141.
31 K. Zhou, Z. Yang and S. Yang, ***Chem. Mater.,*** 2007, 19, 1215-1217.

32　K. C. Chin, G. L. Chong, C. K. Poh, L. H. Van, C. H. Sow, J. Lin and A. T. S. Wee, *J. Phys. Chem. C*, 2007, **111,** 9136-9141.

33　H. Zhang, W. Li, M. Jin, J. Zeng, T. Yu, D. Yang, Y. Xia, *Nano Lett.,* 2010, **11,** 898-903.

5　34　J. Park, J. Joo, S. G. Kwon, Y. Jang and T. Hyeon, *Angew. Chem. Int. Ed.,* 2007, **46**, 4630-4660.

35　J. Polte, T. T. Ahner, F. Delissen, S. Sokolov, F. Emmerling, A. F. Thünemann and R. Kraehnert, *J. Am. Chem. Soc.,* 2010, **132,** 1296-1301.

10　36　N. J. J. Johnson, A. Korinek, C. Dong and F. C. J. M. van Veggel, *J. Am. Chem. Soc.,* 2012, **134,** 11068-11071.

37　 F. Li, W. C. Yoo, M. B. Beernink, A. Stein, *J. Am. Chem. Soc.,* 2009, **131,** 18548-18555.

38　M. J. Fernandez-Merino, L. Guardia, J. I. Paredes, S. Villar-Rodil, A.
15　Martinez-Alonso and J. M. D. Tascon, *RSC Adv.,* 2013, **3,** 18323-18331.

39　F. Lin and R. Doong, *J. Phys. Chem. C* 2011, **115**, 6591-6598.

40　X. Zhang, Z. Su, *Adv. Mater.,* 2012, **24,** 4574-4577.